Absolute quantification of perfusion by dynamic susceptibility contrast MRI using Bookend and VASO steady-state CBV calibration: a comparison with pseudo-continuous ASL.

Lind, Emelie; Wirestam, Ronnie; Markenroth Bloch, Karin; Ahlgren, André; van Osch, Matthias J P; van Westen, Danielle; Surova, Yulia; Ståhlberg, Freddy; Knutsson, Linda

Published in:
Magma

DOI:
10.1007/s10334-014-0431-x

2014

Absolute quantification of perfusion by dynamic susceptibility contrast MRI using Bookend and VASO steady-state CBV calibration: a comparison with pseudo-continuous ASL

Emelie Lindgren[1], Ronnie Wirestam[1], Karin Markenroth Bloch[1,2], André Ahlgren[1], Matthias J.P. van Osch[3], Danielle van Westen[4,5], Yulia Surova[6,7], Freddy Ståhlberg[1,5,8] and Linda Knutsson[1]

[1]Department of Medical Radiation Physics, Lund University, Lund, Sweden

[2]Clinical science, Philips Healthcare, Lund, Sweden

[3]C.J.Gorter Center for high field MRI, Department of Radiology, LUMC, Leiden, Netherlands

[4]Center for Medical Imaging and Physiology, Skåne University Hospital Lund, Lund, Sweden

[5]Department of Diagnostic Radiology, Lund University, Lund, Sweden

[6]Department of Clinical Sciences, Lund University, Lund, Sweden

[7]Department of Neurology, Skåne University Hospital, Lund, Sweden

[8]Lund University Bioimaging Center, Lund University, Lund, Sweden

Correspondence to:

Emelie Lindgren
Department of Medical Radiation Physics
Lund University Hospital
22185 Lund, Sweden

E-Mail: Emelie.Lindgren@med.lu.se
Telephone: +46 46 173146
Fax: +46 46 178540

Keywords: Cerebral blood flow, VASO, BOOKEND, DSC-MRI, perfusion

Abstract

Objective: Dynamic susceptibility-contrast MRI (DSC-MRI) tends to return elevated estimates of cerebral blood flow (CBF) and cerebral blood volume (CBV). In this study, subject-specific calibration factors (CFs), based on steady-state CBV measurements, were applied to rescale the absolute level of DSC-MRI CBF.

Materials and Methods: Twenty healthy volunteers were scanned in a test-retest approach. Independent CBV measurements, for calibration, were accomplished using a T1-based contrast agent steady-state method (referred to as Bookend) as well as a blood-nulling vascular space occupancy (VASO) approach. Calibrated DSC-MRI was compared with pseudo-continuous arterial spin labeling (pCASL).

Results: For segmented grey matter (GM) regions of interests (ROIs), pCASL-based CBF was 63±11 ml/(min100g) (mean±SD). Nominal CBF from non-calibrated DSC-MRI was 277±61 ml/(min100g), while calibrations resulted in 56±23 ml/(min100g) (Bookend) and 52±16 ml/(min100g) (VASO). Calibration tended to eliminate the overestimation, although the repeatability was, generally, moderate and the correlation between calibrated DSC-MRI and pCASL was low ($r<0.25$). However, using GM instead of WM ROIs for extraction of CFs resulted in improved repeatability.

Conclusion: Both calibration approaches provided reasonable absolute levels of GM CBF, although the calibration methods suffered from low signal-to-noise ratio, resulting in weak repeatability and difficulties in showing high degrees of correlation with pCASL measurements.

Introduction

Dynamic susceptibility contrast MRI (DSC-MRI) can provide maps of cerebral blood flow (CBF), cerebral blood volume (CBV) and mean transit time (MTT). DSC-MRI perfusion estimates are generally regarded to be reliable in relative terms, but both CBF and CBV values have tended to be overestimated [1]. Although relative maps of perfusion and perfusion-related parameters are often sufficient, there are applications for which absolute values are warranted, for example for diagnostics and follow-up of patients with stroke, intracranial tumour, dementia and depression [2-6]. One feasible approach to obtain reliable absolute values is to measure CBV with a complementary method that provides absolute values, either globally or locally, and to compare these values with the corresponding DSC-MRI CBV estimates to determine a calibration factor (CF).

In the previously proposed Bookend method [7,8], CBV is estimated using steady-state measurements of T1 before and after contrast agent (CA) administration to determine the CF. The Bookend method has previously been compared to positron emission tomography (PET), which is commonly regarded as the gold standard method for CBF measurements, and a good correlation between the two methods was observed [9]. Another method for absolute CBV estimation is vascular space occupancy (VASO), where a sequence for nulling of the signal from pre-CA blood is used before and after administration of CA [10]. In the present study, steady-state CBV measurements from pre- and post-CA T1 measurements (for the Bookend approach) as well as from the VASO method were used to calibrate CBF from DSC-MRI in a test-retest study in 20 healthy subjects, and the results were compared to CBF from pseudo-continuous arterial spin labeling (pCASL). Absolute CBF values from pCASL have previously shown reasonable agreement with reference methods such as PET [11,12], and a comparison between pCASL and calibrated DSC-MRI is thus of relevance. The VASO- and Bookend-calibrated CBF estimates were also mutually compared and the repeatability of the measurements was investigated.

Material and Methods

Theory

Dynamic susceptibility contrast-MRI

The original CBV estimates obtained by DSC-MRI are given by Eq. 1 [1]:

$$CBV_{DSC} = \frac{1}{\rho} \cdot \frac{1 - Hct_{LV}}{1 - Hct_{SV}} \cdot \frac{\int_0^\infty C(t)dt}{\int_0^\infty AIF(t)dt} \quad (1)$$

where C(t) is the CA concentration curve in tissue and AIF(t) is the CA concentration curve in a tissue-feeding artery. The original DSC-MRI CBF estimates are given by the relation between C(t), AIF(t) and the tissue impulse residue function R(t), according to [1]:

$$\frac{1}{\rho} \cdot \frac{1 - Hct_{LV}}{1 - Hct_{SV}} \cdot C(t) = CBF_{DSC} \cdot R(t) \otimes AIF(t) \quad (2)$$

where ρ is the density of brain tissue, and Hct_{LV} and Hct_{SV} are the hematocrit levels in large and small vessels, respectively, and "⊗" denotes convolution, i.e., CBF_{DSC} can be obtained by deconvolution.

Bookend concept

According to the Bookend concept, CBV can be obtained from T1 measurements before and after CA administration using the following equations [7,13]:

$$CBV^{FastEx}_{Bookend,tissue} = 100 \cdot \frac{1}{\rho} \cdot \frac{1 - Hct_{LV}}{1 - Hct_{SV}} \cdot \frac{\left(\frac{1}{T1_{post}} - \frac{1}{T1_{pre}}\right)_{Tissue}}{\left(\frac{1}{T1_{post}} - \frac{1}{T1_{pre}}\right)_{Blood}} \quad (3)$$

$$CBV_{Bookend,tissue} = WCF(\Delta R_1) \cdot CBV^{FastEx}_{Bookend,tissue} \quad (4)$$

$CBV^{FastEx}_{Bookend,tissue}$ refers to either the white matter (WM) or the grey matter (GM) steady-state CBV, and $T1_{post}$ and $T1_{pre}$ are the T1 values after and before administration of CA, respectively. Eq. 3 assumes fast water exchange between the intra- and the extra-vascular space [14,15], and WCF(ΔR_1) corrects for expected deviations from the fast-water-exchange limit [7]. The WCF is dependent on the concentration of CA in blood as well as on sequence parameters in the T1 measurements and can be obtained by fitting a curve, of the form $a\cdot\Delta R_1^2+b\cdot\Delta R_1+c$ to $CBV_{true,tissue}/CBV^{FastEx}_{Bookend,tissue}$ data plotted as a function of the change in longitudinal relaxation rate, $\Delta R1$, in blood [7,16].

VASO

For absolute CBV estimation using VASO, a sequence with an inversion time (TI) assumed to null the pre-CA blood signal is employed, before and after CA administration [10]. Since the T1 of blood, but not of the extravascular space in tissue (in case of intact BBB), is changed by the CA, the difference between images acquired before and after CA administration is proportional to CBV. The relation can be expressed as follows [10]:

$$CBV_{VASO} = 100 \cdot \frac{1}{\rho} \cdot \frac{S_{post} - S_{pre}}{A \cdot C_b} \cdot \frac{1}{K_{slices}} \quad (5)$$

S_{post} and S_{pre} are the tissue signals in images after and before CA, respectively, and $A\cdot C_b$ corresponds to the signal in blood in the post-CA images. K_{slices} is a factor that corrects for the fact that only one slice can experience exactly the desired inversion time. The K_{slices} factors can be calculated according to $K_{slices} = 2 \cdot e^{-\frac{TI_{slice}}{T1_{blood}}}$ where TI_{slice} is the actual inversion time for each slice and $T1_{blood}$ is T1 in blood before CA.

Calibration of DSC-MRI

Assuming that MTT is correctly measured by DSC-MRI, the same CF can, in principle, be used to calibrate both CBF and CBV estimates since MTT=CBV/CBF (according to the central volume theorem). CFs were estimated according to Eq. 6:

$$CF = \frac{CBV_{reference}}{CBV_{DSC}} \quad (6)$$

where $CBV_{reference}$ refers to $CBV_{Bookend}$ or CBV_{VASO}. In this study, the CFs were applied to CBF data only, and absolute CBF maps were obtained as follows:

$$CBF = CBF_{DSC} \cdot CF \quad (7)$$

Pseudo-continuous arterial spin labelling

The magnetization difference ΔM (control – label) was modeled as follows [17,18]

$$\Delta M = 2 \cdot M0_a \cdot \alpha \cdot CBF \cdot T1_a \cdot (1 - e^{-\tau/T1_a}) \cdot e^{-w/T1_a} \quad (8)$$

where a is the total labeling efficiency (including loss of label due to background suppression inversion pulses), $T1_a$ is T1 of arterial blood, τ is the labeling duration and w is a slice-specific post-label delay given by $w = w_{ps} + (n_{slice} - 0.5) \cdot t_{ro}$, where w_{ps} is the preset post-label delay, n_{slice} is the slice number and t_{ro} is the slice readout time. $M0_a$ is the equilibrium magnetization, given by:

$$M0_a = \frac{S_{WM}}{1 - e^{-TR_{ref}/T1_{WM}}} \cdot \frac{\lambda_a}{\lambda_{WM}} \cdot \frac{e^{-TE/T2^*_a}}{e^{-TE_{ref}/T2^*_{WM}}} \cdot \rho \quad (9)$$

where S_{WM} is the signal intensity of WM in a reference scan, used as a calibration standard, λ_i is the fractional volume water content of compartment i, TR_{ref} and TE_{ref} are the repetition time and echo time respectively of the reference scan and $T2^*_i$ is the effective transverse relaxation time of compartment i.

Subjects and measurements

All measurements were performed using a 3T MRI unit (Philips Achieva, Philips Healthcare, Best, The Netherlands) with approval from the Regional Ethical Review Board in Lund, Sweden, and with written informed consent obtained from each volunteer. Twenty healthy volunteers (ten females and ten males divided into two equally sized age groups, 25-34 years and 51-84 years, respectively) were scanned two times with 7-20 days between investigations. To ensure that all volunteers were healthy and could be expected to show normal CBF, each volunteer participated in a neurological physical examination, including basic cognitive testing, and the volunteers were also asked not to drink any coffee during the day of the examinations. No volunteer used

prescription drugs potentially influencing CBF. The CA (Dotarem, Guerbet, Paris, France) was injected at a rate of 5 ml/s at a total dose of 0.12 mmol/kg body weight, where 0.02 mmol/kg body weight was injected as a pre-bolus (not used in this study) and 0.1 mmol/kg body weight was injected as the main bolus used for the DSC-MRI experiment. The injections of CA were followed by a saline flush injected at the same rate.

Images for T1 measurements, VASO and DSC-MRI were acquired using the same matrix sixe of 128x128 and field of view of 220×220 mm^2. For pCASL, a matrix size of 96×96 was used for the same field of view. The slice thickness for all images, except for the T1 measurements, was 5 mm with 1 mm slice gap between slices. For the T1 measurement, a three-dimensional (3D) sequence was employed, and a slice thickness of 6 mm and no slice gap was used in order for the images to be comparable to the other protocols. To simplify comparisons, *Smart-Exam* [19] was used for planning of slice orientation and field of view. The timing of the different sequences included in this study can be seen in Table 1.

Dynamic susceptibility-contrast MRI: For DSC-MRI, a single-shot gradient-echo EPI sequence with echo time (TE) 29 ms, flip angle (FA) 60° and SENSE=2.5 was used to cover an imaging volume of 20 slices during 87 seconds, including the first passage of CA, at a temporal resolution of 1243 ms.

T1 measurement: T1 quantification was accomplished using a 3D Look-Locker sequence [20], providing signal data from 16 time points after an adiabatic inversion pulse with 200 ms time intervals, a repetition time (TR) of 10 seconds, FA=5° and TE=3.5 ms. Twelve slices were collected using an EPI-factor (EPI echoes per excitation) of three and a TFE-factor (echoes per excitation in a turbo spin echo) of nine.

Vascular space occupancy: In the VASO data acquisition, ten slices were collected (separated 13 ms in time) using a blood-nulling sequence with TR=6 s, TE=6 ms, TI=1088 ms for the first slice and a global inversion pulse [10]. A segmented EPI with EPI-factor nine was used and both magnitude and phase images were obtained.

Pseudo-continuous arterial spin labelling: For pCASL, 16 slices were collected using 30 repetitions, with TE=14 ms, TR=4000 ms, FA=90°, EPI-factor 37 and SENSE=2.3. The label duration was 1650 ms, the post label delay 1600 ms and the label gap 20 mm. Background suppression was used with TIs 1710 and 2860 ms. A separate sequence for reference measurement of M0 was applied using the same parameters as in the pCASL

sequence, except for the use of TR=10000 ms, four repetitions and no background suppression. An image of the labelling plane from the first investigation was used as a guide for positioning of the labelling plane at the second investigation.

Post-processing

In this study, individual global CFs were estimated, for each investigation, to calculate quantitative CBF maps from DSC-MRI. Since DSC-MRI is considered to provide reliable relative values, global CFs can be used which ensures higher SNR than CFs extracted locally or pixel by pixel. Two approaches, using either WM or GM ROIs for the extraction of CFs, were applied. WM ROIs can more easily be extracted with minimal partial volume effects, so WM ROIs are often used to provide CFs. However, GM CBV is higher, so GM ROIs can be expected to show higher SNR for the CBV estimations.

Dynamic susceptibility-contrast MRI

CBF_{DSC} and CBV_{DSC} were calculated according to Eqs. 1-2, using ρ=1.04 g/ml, Hct_{LV}=0.45 and Hct_{SV}=0.25 [21]. Global AIFs were obtained by averaging 4-8 semi-automatically identified local AIFs, and the deconvolution was carried out using a block-circulant singular value decomposition algorithm [22] using 10% of the maximum singular value as a fixed cut off level.

Bookend

Images from the 3D Look-Locker sequence were processed by *MRmap* [23] for calculation of T1 maps, and $CBV_{Bookend}$ was subsequently calculated using Eqs. 3 and 4 by first calculating the mean value of $T1_{pre}$ and $T1_{post}$ in the ROIs used for estimation of calibration factors (further described below). The three pixels in the volume showing the highest difference in relaxation rate between pre- and post-CA administration in the sagittal sinus were selected to represent blood. To avoid noise effects the selected pixels were also required to show high signal (i.e., being among the 3% of the voxels with the highest signal) at the last time point in the post-CA images from the Look-Locker sequence. $CBV_{true,WM}$ = 1.91 ml/100g and $CBV_{true,GM}$ = 3.85 ml/100g was used [7] for the estimation of WCF, and the fitting was carried out using a non-linear least square fitting (with zero as lower limit and infinity as upper limit).

VASO

A·Cb was determined as the mean value of three pixels in the sagittal sinus showing the largest signal in the post-CA images. CBV_{VASO} was estimated using Eq. 5 where S_{pre} and S_{post} were calculated as mean values in each slice containing at least 10 pixels of the selected WM and GM ROIs in both pre- and post CA images. (S_{post}-S_{pre}) values were corrected by K_{slices}= [0.95, 0.96, 0.97, 0.98, 0.98, 0.99, 1.00, 1.01, 1.01, 1.02] (assuming $T1_{blood}$=1624 ms [24]). A weighted mean of all slices provided ROI values of CBV_{VASO}. Post-CA images will show higher signal compared with the pre-CA situation since blood will also contribute to the post-CA signal. A voxel including compartments with long T1 (e.g., CSF) might show negative signal, due to the inversion time used, and higher signal will thus be interpreted as a signal loss in the magnitude images. To take this effect into account, the magnitude data were sign corrected using phase images before Eq. 5 was utilized. VASO phase images were unwrapped and high-pass filtered, and voxels showing phase values $-90° \leq \varphi < 90°$ and $90° \leq \varphi < 270°$ were set to show positive and negative signal, respectively [25] (except in one dataset, where phase images were unavailable).

Calibration factors

For extraction of an individual (either WM- or GM-based) global CF for each investigation, $CBV_{Bookend}$, CBV_{VASO} and CBV_{DSC} were estimated in WM as well as GM ROIs. The ROIs were extracted in the following way: Pre- and post-CA T1 images ($T1_{pre}$ and $T1_{post}$) were matched to each other and coregistered to the first time point in the DSC-MRI time series (DSC_{first}). Pre- and post-CA VASO images ($VASO_{pre}$ and $VASO_{post}$) were matched to each other and coregistered to DSC_{first} using the same procedure. Using *new segment* in SPM8 [www.fil.ion.ucl.ac.uk/spm], segmentations of WM and GM were performed on coregistered $T1_{pre}$ and on DSC_{first} images creating tissue probability maps (one for each tissue type) with values from 0 to 1 indicating the fraction of the voxel containing the tissue of interest. Voxels with values exceeding two times the global mean CBV_{DSC} value were assumed to represent large vessels and were excluded from the DSC_{first} WM and GM segmentation. A segmentation threshold of 0.55 was used for both WM and GM to create binary ROIs (where thresholds were chosen after visual inspection of some datasets to provide ROIs of reasonable size) and a common ROI was created, including only voxels for which *both* $T1_{pre}$ and DSC_{first} showed the binary value 1. $T1_{pre}$ was chosen for segmentation purposes due to superior contrast, and the additional requirement of an

overlap between $T1_{pre}$ and DSC_{first} regions was introduced to minimize effects of EPI-readout-related distortions in the DSC-MRI images. The resulting ROI was transferred to the space of the original T1 and VASO images by applying an inverse reslice operation (with parameters obtained from the co-registration). This ROI transfer introduced some degree of smoothing, so the ROIs were thresholded (typically at 0.5) to give the same ROI size as for the common ROI in the creation of binary ROIs after the inverse reslice operation. CFs were then estimated according to Eq. 6 and used for calculation of quantitative CBF values using Eq. 7.

Pseudo-continuous arterial spin labeling

S_{WM}, (cf. Eq. 9) was estimated from a binary WM mask automatically produced for each subject by thresholding the segmented WM tissue probability map at 0.95 using SPM [www.fil.ion.ucl.ac.uk/spm] and perfusion values were calculated using Eq. 8. The parameters α, $T1_a$, λ_a, λ_{WM}, $T2^*_a$, $T2^*_{WM}$, and ρ were taken from the literature as 70% [26], 1.65 s [24], 87% [27], 73% [27], 43.6 ms [28], 44.7 ms [21] and 1.04 g/ml [21], respectively.

Comparison of CBF estimates from calibrated DSC-MRI and pCASL

For comparison of calibrated DSC-MRI results with the corresponding pCASL data, values of CBF were extracted in a new set of GM ROIs (not identical to the ones used for calibration). DSC_{first} and calculated pCASL CBF maps were coregistered to the M0 images from the pCASL experiment, and segmentation of GM was performed in *new segment* in SPM8 [www.fil.ion.ucl.ac.uk/spm] based on the M0 images for pCASL and the coregistered DSC_{first} for DSC-MRI, creating probability maps of GM. A threshold of 0.55 was used to create binary ROIs and a common ROI was created, including only voxels for which both data sets showed the binary value 1. An inverse reslice operation of the ROI was performed for the DSC_{first} and pCASL images to obtain the common ROI in the DSC_{first} and pCASL space. To get binary ROIs, a threshold was applied to create ROIs of approximately the same size as before the inverse reslice operation. Voxels with values exceeding two times the global mean CBF_{DSC} value were excluded from the GM ROIs in DSC-MRI in order to avoid contribution from large vessels.

Four investigations in three different volunteers were excluded due to pCASL scans with non-optimal labeling, leading to unrealistically low CBF values and inhomogeneous CBF maps. For volunteers where one of the

investigations was excluded, the single value of the successful investigation was used instead of the mean value of visit 1 and visit 2 for comparison with DSC-MRI.

Statistical analysis

For CBF test-retest analysis and for comparison of CBF estimates, Bland-Altman analyses [29] were carried out. For the comparison between DSC-MRI (calibrated and non-calibrated) and pCASL, and for the mutual comparison between Bookend- and VASO-calibrated DSC-MRI, the mean value of visit 1 and visit 2 was used and the standard deviations (SDs) in the Bland-Altman analyses were thus corrected according to $SD_C = \sqrt{SD_m{}^2 + 0.25 \cdot SD_{m1}^2 + 0.25 \cdot SD_{m2}^2}$ [29], where SD_m is the SD of the differences between method 1 and method 2 (using the mean value of visit 1 and visit 2 for each method), while SD_{m1} and SD_{m2} are the SDs of the differences between visit 1 and visit 2 for method 1 (m1) and method 2 (m2), respectively. For completeness, linear correlation analyses were included for comparisons of datasets which were expected to show linear relationships.

Results

The fitting of $CBV_{true}/CBV_{Bookend}^{FastEx}$ versus the change in ΔR1 in blood gave the WCF expression $WCF(\Delta R_1) = 5.1 \cdot 10^{-7} \cdot \Delta R_1^2 + 0.56 \cdot \Delta R_1 + 0.61$ for WM and $WCF(\Delta R1) = 0.24 \cdot \Delta R_1^2 + 3.3 \cdot 10^{-8} \cdot \Delta R_1 + 1.7$ for GM. Estimated $CBV_{Bookend}^{FastEx}$ (without correction for water-exchange-effects) and CBV_{true}/WCF (where WCF is given by the fitted function) can be seen in Figure 1.

Figure 2 shows the repeatability of the $CBV_{reference}$ measurements used for determining the CFs for Bookend and VASO. The correlation coefficients from the linear regressions were generally low, for both Bookend and VASO, indicating uncertainties in the CBV estimation.

A summary of the mean values of GM CBF is given in Table 2, showing a clear overestimation of CBF from non-calibrated DSC-MRI when compared with pCASL as well as both Bookend- and VASO-calibrated DSC-MRI. Figure 3 and Figure 4 show the repeatability of Bookend- and VASO-calibrated GM CBF, illustrated using scatter plots as well as Bland-Altman diagrams, and the corresponding repeatability of GM CBF obtained by pCASL is also shown. When using WM ROIs (Figure 3) for calibration, the repeatability study for both Bookend and VASO calibration resulted in low correlation coefficients in the scatter plots and large SDs in the Bland-Altman plots. The test-retest data for calibration based on GM ROIs (Figure 4) showed improved repeatability, most clearly seen as reduced SDs in the Bland-Altman plots for both Bookend and VASO.

Figure 5 and Figure 6 show the comparison of non-calibrated and calibrated DSC-MRI with pCASL. Neither the scatter plots nor the Bland-Altman plots indicated good correspondence between DSC-MRI and pCASL. The use of GM ROIs (Figure 6) instead of WM ROIs (Figure 5) for calibration did not seem to substantially improve the correspondence between the methods. All correlation coefficients were low ($r<0.25$) and the Bland-Altman plots showed large SDs (shown as dotted lines) indicating large differences between the two methods compared. However, the mean values of the differences between DSC-MRI and pCASL (shown as solid lines in the Bland-Altman plots) were close to zero for all calibrated DSC-MRI estimates.

Finally, the CBF estimates from Bookend calibration and VASO calibration were mutually compared. Results using WM ROIs (Figure 7a-b) as well as GM ROIs (Figure 7c-d) for extraction of CFs are shown, and mean values from visit 1 and visit 2 are displayed. Using GM ROIs for calibration, the methods showed fairly good agreement, i.e., small SDs in the Bland-Altman plot and reasonable correlation coefficients (0.88 for GM calibration ROIs).

Discussion

Non-calibrated DSC-MRI has previously tended to show high CBV and CBF estimates compared with PET values [1] and the Bookend technique as well as a VASO sequence can potentially be used for calibration of DSC-MRI with the aim to establish more reliable absolute levels of CBF. In the present study, the comparison between non-calibrated DSC-MRI and pCASL (Figure 5) showed no convincing correspondence, and both the scatter plots and the Bland-Altman analysis showed a large bias with severely overestimated values from DSC-MRI (approximately 4-5 times higher than pCASL). Both calibration techniques returned CBF values that were, on a group level, closer to the pCASL results as well as to literature values typically obtained by other methods such as ASL and PET [30-34]. However, both Bookend and VASO suffered from uncertainties that contributed to variations between visit 1 and visit 2 in the repeatability studies (Figures 3 and 4). Most of the variations seemed to originate from the $CBV_{reference}$ (Figure 2) estimates used for calibration, and various plausible sources of uncertainty will be discussed below.

Estimation of $CBV_{reference}$

One important issue in determining absolute CBV values is that the effect of the CA in pure blood ($\Delta R1$ for Bookend and S_{post} for VASO) has to be known, since these measures act as a direct scaling of all the CBV values. If a selected voxel suffered from partial volume effects, but was assumed to be pure blood, an overestimation of CBV would occur. To reduce random noise effects, which could result in large uncertainties of the estimated $CBV_{reference}$ values, the average of three voxels was used in this study, but measurement noise may still be an issue.

One important reason for the poor $CBV_{reference}$ repeatability in WM is, most likely, the small CA effect in tissue due to a low CBV. In this study, the effect of the CA might have been even smaller than in previous studies since the estimated $\Delta R1$ in blood in this study was 2.2 s^{-1} (at a CA dose of 0.12 mmol/kg), while earlier studies showed values about 2-4 times higher after injection of 0.1 mmol/kg of CA [7,16]. The reason for this is not fully understood, but one possible explanation is that, in our study, a longer time delay between the bolus passage and the post-CA images, acquired at steady-state, were used. A longer time delay might influence the concentration of CA in blood [35] and lead to correspondingly smaller CA effects in tissue. Blood $\Delta R1$ (for Bookend) and S_{post} (for VASO) are used to scale CBV, so lower CA concentrations in blood (and thus in tissue)

are not expected to influence the absolute levels, but will lead to increased uncertainties in the $CBV_{reference}$ estimations. Accordingly, the use of GM ROIs for $CBV_{Bookend}$ estimation gave improved test-retest results compared with WM ROIs. For Bookend, the higher CBV in GM would imply approximately twice as large a ΔR1 change in GM compared with WM (and ΔR1 thus becomes more comparable with previous studies showing higher CA concentration in blood).

Another highly relevant aspect of the uncertainties in $CBV_{reference}$ is subject movement between the pre- and post-CA examinations. Since pre- and post-CA images are to be directly compared, it is important to identify the same tissue volume in the two data sets. One obvious solution would be to perform motion correction during the post-processing of the data. However, smoothing due to interpolation of the corrected images can modify the quantitative pixel values, and this was a substantial concern in the present study where only small differences between pre- and post-CA images were to be expected. Hence, to avoid changing the actual values in the images used for calculations, the approach of correcting the ROIs for motion was used in this study, instead of applying motion correction to the pre- and post-CA images. It should, however, be noted that the employed method is also associated with some problems, for example, interpolation issues within the ROIs which might introduce differences between the ROIs compared. Motion between pre-CA and post-CA images can also affect the estimation of ΔR1 in blood for Bookend, which is difficult to correct for.

For Bookend, the absolute levels of $CBV_{reference}$ are dependent on the assumed value for CBV_{true} used in the curve fitting for estimation of WCF (i.e., higher CBV_{true} would provide higher $CBV_{Bookend}$ and vice versa). The shape of the fitted curve is not critically dependent on the value of CBV_{true} [7], but the absolute $CBV_{reference}$ value, and thereby the calibrated CBF level, is dependent on CBV_{true}. Another potential WCF issue is suboptimal fitting of the curve that provides the WCFs. In this study, ΔR1 in blood did not differ much between subjects. Hence, the fitting of the curve subsequently used to obtain the WCF was rather challenging and, especially for WM ROIs, the fitted curve did not seem to describe the data very well (probably due to larger uncertainties in $CBV^{FastEx}_{Bookend,tissue}$ estimates compared to GM ROIs). However, a quadratic form was used for the fitting procedure in order to comply with the originally proposed methodology [7]. A general weakness of this approach is that the data to be corrected are also used for estimation of WCF, and there is a risk of a circular argument

since, for example, underestimation of ΔR1 in blood would result in a higher $CBV_{Bookend,tissue}^{FastEx}$ according to Eq. 3 which could be interpreted as a water exchange effect and then be corrected for by the WCF.

For VASO, another issue for correct $CBV_{reference}$ estimations in this study is that no subject-specific TI was used for nulling of the blood. Since T1 in blood is known to differ between subjects, for example, due to hematocrit differences, the effectiveness of the blood nulling might be different across volunteers [24]. Since T1 is not expected to vary noticeably between visit 1 and visit 2, this effect is expected to be the same at both visits and is not likely to have impacted the repeatability. However, when comparing VASO-calibrated CBF values with Bookend-calibrated CBF values and with pCASL, this effect might have played a role.

Repeatability of GM CBF

For both Bookend and VASO, the test-retest investigations of calibrated GM CBF values using WM ROIs showed quite large uncertainties in the measurements, probably arising from uncertainties in $CBV_{reference}$ (Figure 2). Bookend Bland-Altman plots showed larger SDs than in a previous test-retest study by Shin et al. [36], who observed an average difference±SD of 1.4±6.9 ml/(min 100g). On the other hand, Crane et al. [37] also had difficulties in showing good repeatability for Bookend-calibrated DSC-MRI. Repeatability was generally improved by the use of GM ROIs for $CBV_{reference}$ estimation, as reflected by the scatter plots (values closer to the identity lines and improved correlation coefficients) and by smaller SDs in the Bland-Altman plots (Figure 4). For the Bookend method, the use of GM ROIs resulted in a repeatability that was fairly similar to the previous observations by Shin et al. [36].

Comparison with pCASL

In the Bland-Altman comparison of the VASO and Bookend methods with pCASL, both calibration approaches showed absolute values which were comparable to pCASL, with a mean difference close to zero using WM ROIs for calibration (Figure 5) and somewhat lower values when using GM ROIs for calibration (Figure 6). However, the SDs were quite large and the correlation coefficients from the linear fits of DSC-MRI CBF versus pCASL CBF were low (Figures 5 and 6). One obvious problem is that the calibration methods suffered from uncertainties (shown in the repeatability studies), leading to difficulties in establishing a clear correspondence

with another method, and a small range of values to be compared also hampers visualization of the degree of correspondence in a scatter plot. Another issue when comparing pCASL and DSC-MRI is potential geometric distortions in DSC-MRI, related to the use of EPI readout and not present in pCASL. This problem was, however, minimized by only using voxels that were independently defined as GM by the segmentations for both pCASL and DSC-MRI. Due to different in-plane resolutions, the partial volume effects in DSC-MRI and pCASL might have differed. However, the same segmentation threshold was used for both pCASL and DSC-MRI in the ROI selection, i.e., the same maximal fraction of partial volume effects was applied to all included voxels.

As pCASL showed both good repeatability (cf. Figure 3) and reasonable absolute values [31-34], a comparison between calibrated DSC-MRI and pCASL is indeed of interest. Nevertheless, it should be remembered that the value of $M0_a$ scales all the CBF values in a pCASL volume, so the method used to determine $M0_a$ will directly influence the absolute level of CBF. Unfortunately, poor labeling in some of the feeding arteries for some of the scans, led to unrealistically low perfusion estimates in some territories. This is a general disadvantage of the pCASL method, resulting in exclusion of some of the collected data in this study. It is also possible that pCASL measurements inherently reflect a somewhat different aspect of the microcirculation than intravascular CA-based methods.

Bookend versus VASO

Using GM ROIs for calibration, a quite reasonable agreement between Bookend and VASO estimates was observed, both in the scatter plots and the Bland-Altman plots (Figures 7c-d). Despite the poor test-retest CBF results for Bookend and VASO, when calibrated using WM ROIs, the linear fit showed a tendency to a linear relationship between the two methods, although the SDs in the Bland-Altman plot were rather large (Figures 7a-b). However, since the mean values of visit 1 and 2 are used in the comparison, some of the measurement uncertainties are reduced. It is also possible that both calibration methods suffered from the same source of uncertainty, for example, motion between pre- and post-CA scans, which may have influenced the estimated $CBV_{reference}$ values in a similar direction.

Conclusion

Despite the limitations of DSC-MRI, it has the inherent advantages of being readily available in clinical environments and providing not only CBF but also other hemodynamic parameters such as CBV and MTT, therefore a DSC-MRI protocol providing accurate absolute values with acceptable repeatability would thus be of considerable clinical value. In this study, CBV estimates from Bookend and VASO were used to obtain absolute values of CBF in GM. On a group level, absolute CBF values after calibration were reduced to levels comparable to other CBF methods such as PET and pCASL. However, no evident linear relationship between DSC-MRI and pCASL was seen after the calibration procedures. Furthermore, when using WM ROIs to obtain calibration factors, the test-retest results for GM CBF from calibrated DSC-MRI were not convincing, but the use of GM ROIs for calibration improved the repeatability of both methods, indicating that some of the uncertainties might be due to a lower CA concentration in blood compared with previous studies.

Acknowledgements

Thanks to Dr Christian Stehning at Philips Research in Hamburg for providing the sequence for T1 measurements. This study was supported by the Swedish Research Council (Grant Nos. 13514 and no. 2010-4454).

References

1. Knutsson L, Ståhlberg F, Wirestam R (2010) Absolute quantification of perfusion using dynamic susceptibility contrast MRI: pitfalls and possibilities. Magn Reson Mater Phy 23:1-21

2. Baron JC (2001) Perfusion Thersholds in Human Cerebral Ischemia: Historical Perspective and Therapeutic Implicaitons. Cerebrovasc Dis 11:2-8

3. Weber MA, Zoubaa S, Schlieter M, Jüttler E, Huttner HB, Geletneky K, Ittrich C, Lichy MP, Kroll A, Debus J, Giesel FL, Hartmann M, Essig M (2006) Diagnostic performance of spectroscopic and perfusion MRI for distinction of brain tumours. Neurology 66:1899-1906

4. Broich K, Hartmann A, Adam S, Biersack HJ (1989) Regional cerebral blood flow in dementia of Alzheimer's type. J Neural Transm 1:41

5. Ishii K (2002) Clinical application of positron emission tomography for diagnosis of dementia. Ann of Nucl Med 16:515-525

6. Ohgami H, Nagayama H, Akiyoshi J, Tsuchiyama K, Komaki S, Takaki H, Mori H (2005) Contributing factors to changes of cerebral blood flow in major depressive disorder. J Affect Disord 87:57-63

7. Shin W, Cashen TA, Horowitz SW, Sawlani R, Carroll TJ (2006) Quantitative CBV measurement from static T1 changes in tissue and correction for intravascular water exchange. Magn Reson Med 56:138-145

8. Sakaie KE, Shin W, Curtin KR, McCarthy RM, Cashen TA, Carroll TJ (2005) Method for improving the accuracy of quantitative cerebral perfusion imaging. J Magn Reson Imaging 21:512-519

9. Vakil P, Lee JJ, Mouannes-Srour JJ, Derdeyn CP, Carroll TJ (2013) Cerebrovascular Occlusive Disease: Quantitative Cerebral Blood Flow Using Dynamic Susceptibility Contrast MR Imaging Correlates with Quantitative $H_2[^{15}O]$ PET. Radiology 266:879-886

10. Lu H, Law M, Johnson G, Ge Y, van Zijl PC, Helpern JA (2005) Novel approach to the measurement of absolute cerebral blood volume using vascular-space-occupancy magnetic resonance imaging. Magn Reson Med 54:1403-1411

11. Xu G, Rowley HA, Wu G, Alsop DC, Shankaranarayanan A, Dowling M, Christian BT, Oakes TR, Johnson SC (2010) Reliability and precision of pseudo-continuous arterial spin labeling perfusion MRI on 3.0 T and comparison with ^{15}O-water PET in elderly subjects at risk for Alzheimer's disease. NMR Biomed 23:286-293

12. Ye FQ, Berman KF, Ellmore T, Eposito G, van Horn JD, Yan Y, Duyn J, Smith AM, Frank JA, Weinberger DR, McLaughlin AC (2000) $H_2{}^{15}O$ PET Validation of Steady-State Arterial Spin Tagging Cerebral Blood Flow Measurements in Humans. Magn Reson Med 44:450-456

13. Kuppusamy K, Lin W, Cizek GR, Haacke EM (1996) In vivo regional cerebral blood volume: quantitative assessment with 3D T1-weighted pre- and postcontrast MR imaging. Radiology 201:106-112

14. Hazlewood CF, Chang DC, Nichols BL, Woessner DE (1974) Nuclear magnetic resonance transverse relaxation times of water protons in skeletal muscle. Biophys J 14:583-606

15. Donahue KM, Weisskoff RM, Chesler DA, Kwong KK, Bogdanov AA Jr, Mandeville JB, Rosen BR (1996) Improving MR quantification of regional blood volume with intravascular T1 contrast agents: Accuracy, precision, and water exchange. Magn Reson Med 36:858-867

16. Srour JM, Shin W, Shah S, Sen A, Carroll TJ (2011) SCALE-PWI: A pulse sequence for absolute quantitative cerebral perfusion imaging. J Cereb Blood Flow Metab 31:1272-1282

17. Alsop DC, Detre JA (1996) Reduced Transit-Time Sensitivity in Noninvasive Magnetic Resonance Imaging of Human Cerebral Blood Flow. J Cereb Blood Flow Metab 16:1236-1249

18. Wang J, Alsop DC, Li L, Listerud J, Gonzalez-At JB, Schnall MD, Detre JA (2002) Comparison of quantitative perfusion imaging using arterial spin labeling at 1.5 and 4.0 Tesla. Magn Reson Med 48:242-254

19. Young S, Bystrov D, Netsch T, Bergmans R, van Muiswinkel A, Visser F, Springorum R, Gieseke J (2006) Automated planning of MRI neuro scans. In: Proceedings of the SPIE 6144 on Medical Imaging (Image Processing), San Diego, 61441M

20. Look DC, Locker DR (1970) Time saving in measurement of NMR and EPR relaxation times. Rev Sci Instrum 41:250-251

21. Rempp KA, Brix G, Wenz F , Becker CR , Gückel F, Lorenz WJ (1994) Quantification of regional cerebral blood flow and volume with dynamic susceptibility contrast-enhanced MR imaging. Radiology 193:637-641

22. Wu O, Østergaard L, Weisskoff RM, Benner T, Rosen BR, Sorensen AG (2003) Tracer arrival timing-insensitive technique for estimating flow in MR perfusion-weighted imaging using singular value decomposition with a block-circulant deconvolution matrix. Magn Reson Med 50:164-174

23. Messroghli DR, Rudolph A, Abdel-Aty H, Wassmuth R, Kühne T, Dietz R, Schulz-Menger J (2010) An open-source software tool for the generation of relaxation time maps in magnetic resonance imaging. BMC Med Imaging 10:16

24. Lu H, Clingman C, Golay X, van Zijl PC (2004) Determining the longitudinal relaxation time (T1) of blood at 3.0 Tesla. Magn Reson Med 52:679-682

25. Uh J, Lewis-Amezcua K, Varghese R, Lu H (2009) On the measurement of absolute cerebral blood volume (CBV) using vascular-space-occupancy (VASO) MRI. Magn Reson Med 61:659-667

26. van Osch MJ, Teeuwisse WM, van Walderveen MA, Hendrikse J, Kies DA, van Buchem MA (2009) Can arterial spin labeling detect white matter perfusion signal? Magn Reson Med 62:165-173

27. Donahue MJ, Lu H, Jones CK, Edden RA, Pekar JJ, van Zijl PC (2006) Theoretical and experimental investigation of the VASO contrast mechanism. Magn Reson Med 56:1261-1273

28. Cavuşoğlu M, Pfeuffer J, Uğurbil K, Uludağ K (2009) Comparison of pulsed arterial spin labeling encoding schemes and absolute perfusion quantification. Magn Reson Imaging 27:1039-1045

29. Bland JM, Altman DG (1986) Statistical methods for assessing agreement between two methods of clinical measurement. Lancet 327:307-310

30. Petersen ET, Mouridsen K, Golay X, all named co-authors of the Quasar test-retest study (2010) The QUASAR reproducibility study, Part II: Results from a multi-center Arterial Spin Labeling test-retest study. Neuroimage 49:104-113

31. Leenders KL, Perani D, Lammertsma AA, Heather JD, Buckingham P, Healy MJR, Gibbs JM, Wise RJS, Hatazawa J, Herold S, Beaney RP, Brooks DJ, Spinks T, Rhodes C, Frackowiak RSJ, Jones T (1990) Cerebral blood flow, blood volume and oxygen utilization. Normal values and effect of age. Brain 113:27-47

32. Meltzer CC, Cantwell MN, Greer PJ, Ben-Eliezer D, Smith G, Frank G, Kaye WH, Houck PR, Price JC (2000) Does cerebral blood flow decline in healthy aging? A PET study with partial-volume correction. J Nucl Med 41:1842-1848

33. Ito H, Kanno I, Ibaraki M, Hatazawa J, Miura S (2003) Changes in human cerebral blood flow and cerebral blood volume during hypercapnia and hypocapnia measured by positron emission tomography. J Cereb Blood Flow Metab 23:665-670

34. Yamaguchi T, Kanno I, Uemura K, Shishido F, Inugami A, Ogawa T, Murakami M, Suzuki K (1986) Reduction in regional cerebral metabolic rate of oxygen during human aging. Stroke 17:1220-1228

35. Larsson HBW, Fritz-Hansen T, Rostrup E, Søndergaard L, Ring P, Henriksen O (1996) Myocardial perfusion modeling using MRI. Magn Reson Med 35:716-726

36. Shin W, Horowitz S, Ragin A, Chen Y, Walker M, Carroll TJ (2007) Quantitative cerebral perfusion using dynamic susceptibility contrast MRI: evaluation of reproducibility and age- and gender-dependence with fully automatic image postprocessing algorithm. Magn Reson Med 58:1232-1241

37. Crane DE, Donahue MJ, Chappell MA, Sideso E, Handa A, Kennedy J, Jezzard P, MacIntosh BJ (2013) Evaluating quantitative approaches to dynamic susceptibility contrast MRI among carotid endarterectomy patients. J Magn Reson Imaging 37:936-943

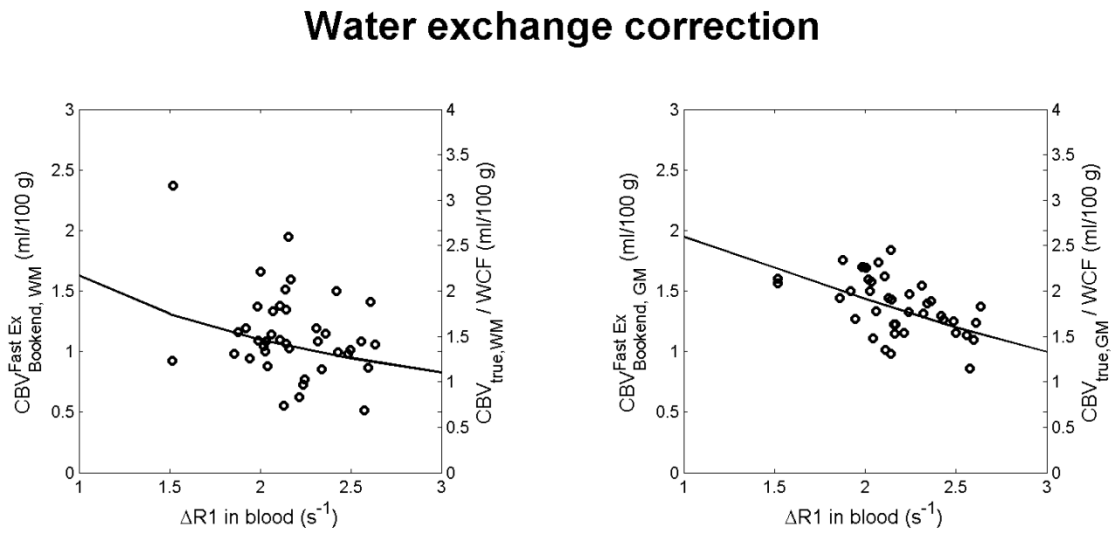

Fig. 1 Curve fitting used to extract the water correction factor (WCF). Circular markers indicate $CBV_{Bookend}^{FastEx}$(scale indicated by the y-axis to the left) in (a) WM ROIs and (b) GM ROIs, plotted as a function of ΔR1 in blood. The solid lines are CBV_{true}/WCF (scale indicated by the y-axis to the right), where WCF was established from fitting a second-order polynomial to CBV_{true}/ $CBV_{Bookend}^{FastEx}$

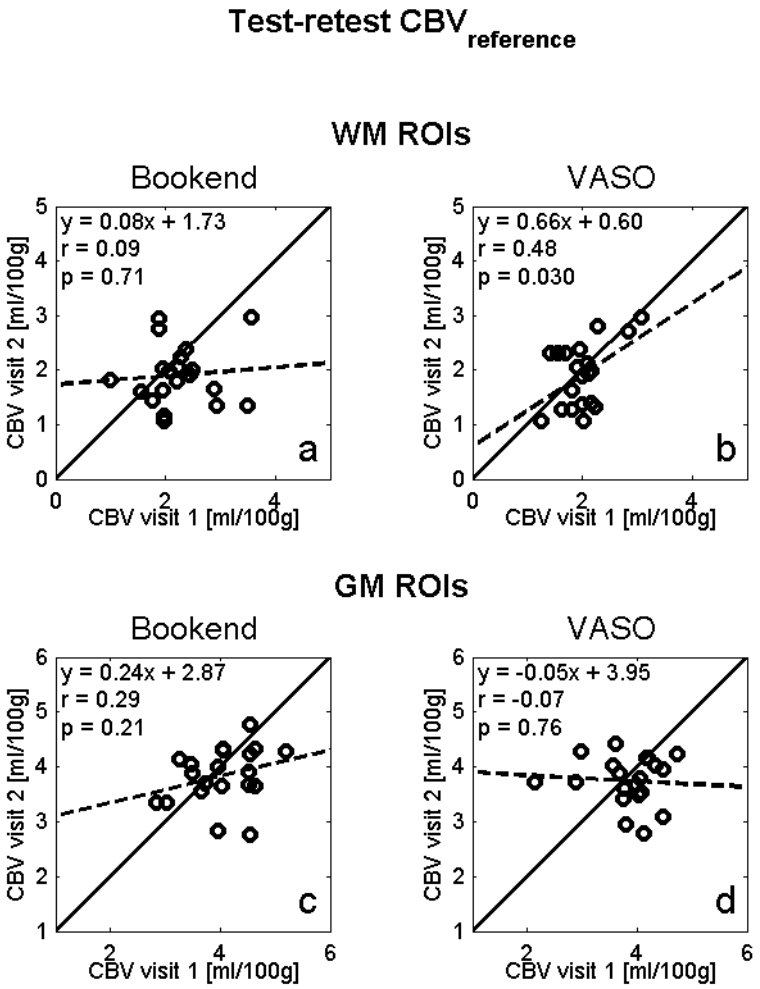

Fig. 2 Test-retest results for (a) $CBV_{Bookend,WM}$ (b) $CBV_{VASO,WM}$ (c) $CBV_{Bookend,GM}$ and (d) $CBV_{VASO,GM}$ used as $CBV_{reference}$ for extracting the DSC-MRI calibration factors. The solid lines show the identity line and the dotted lines show the results from linear regression

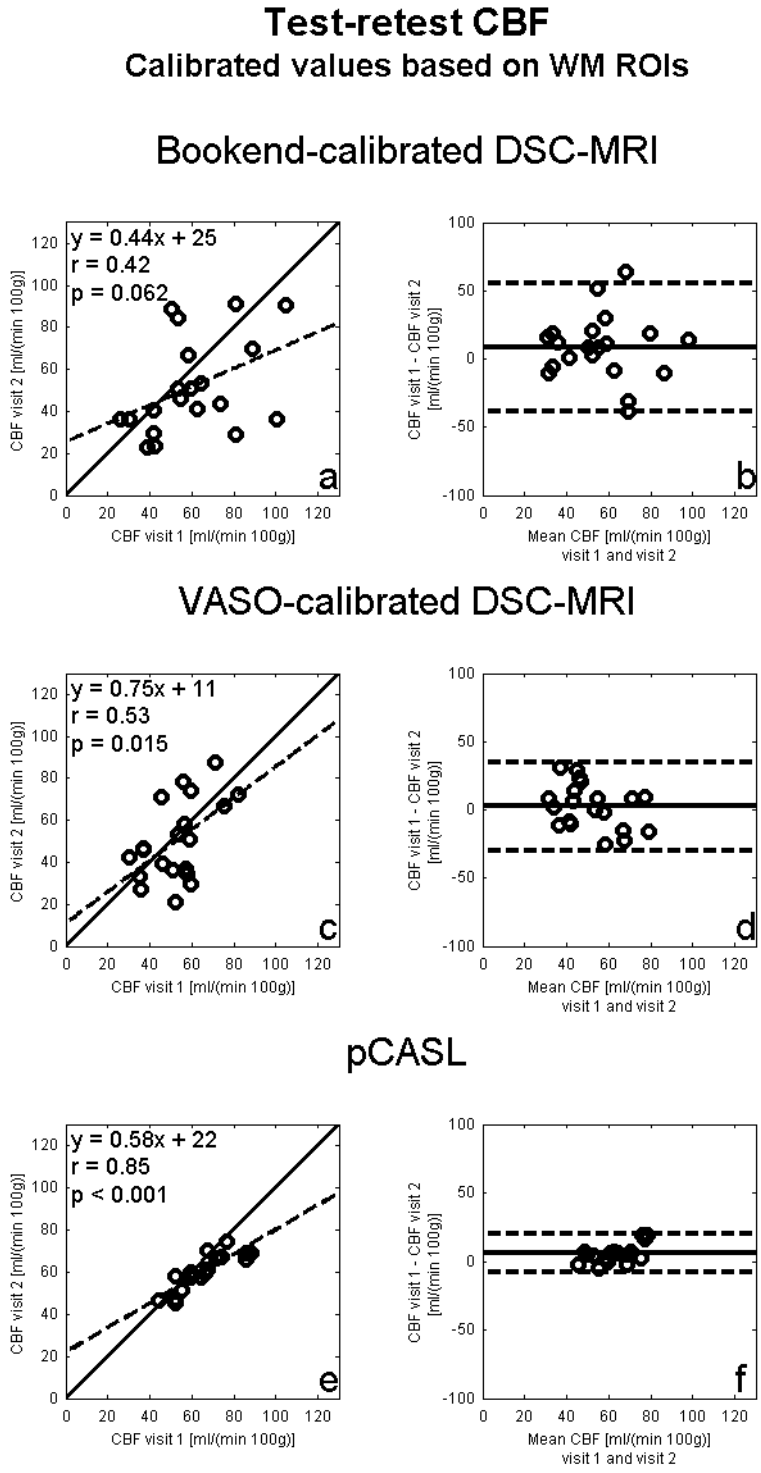

Fig. 3 Test-retest results for GM CBF from DSC-MRI, calibrated using Bookend and VASO, and for GM CBF from pCASL. Calibration is based on $CBV_{reference}$ from WM ROIs. The solid lines in the scatter plots show the identity line and the dotted lines show results from the linear regression. In the Bland-Altman plots, the solid lines shows the mean difference between the first and second visit and the dotted lines show mean±1.96·SD

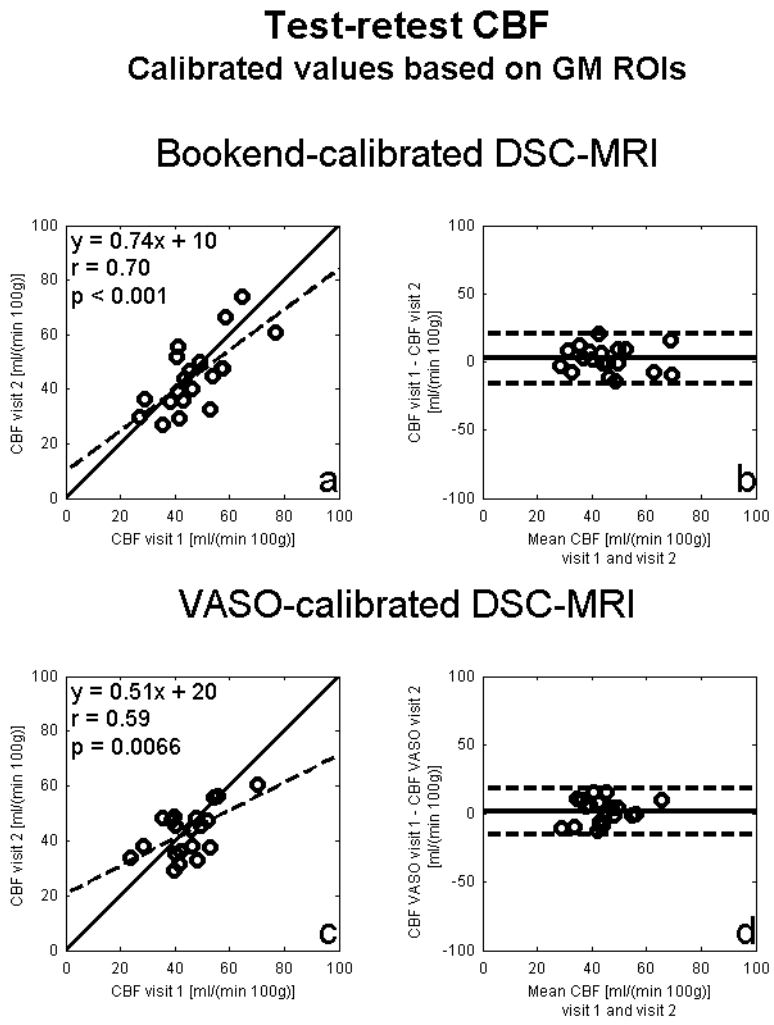

Fig. 4 Test-retest results for GM CBF from Bookend- and VASO-calibrated DSC-MRI. The ROIs for extracting GM CBF values are the same as in Figure 3, but the ROIs for extracting calibration factors are based on $CBV_{reference}$ from GM ROIs. Solid lines in the scatter plots indicate the identity line and dotted lines indicate the results from the linear regression. In the Bland-Altman plots, the solid lines represents the mean value of the differences between visit 1 and visit 2 and the dotted lines show mean±1.96·SD

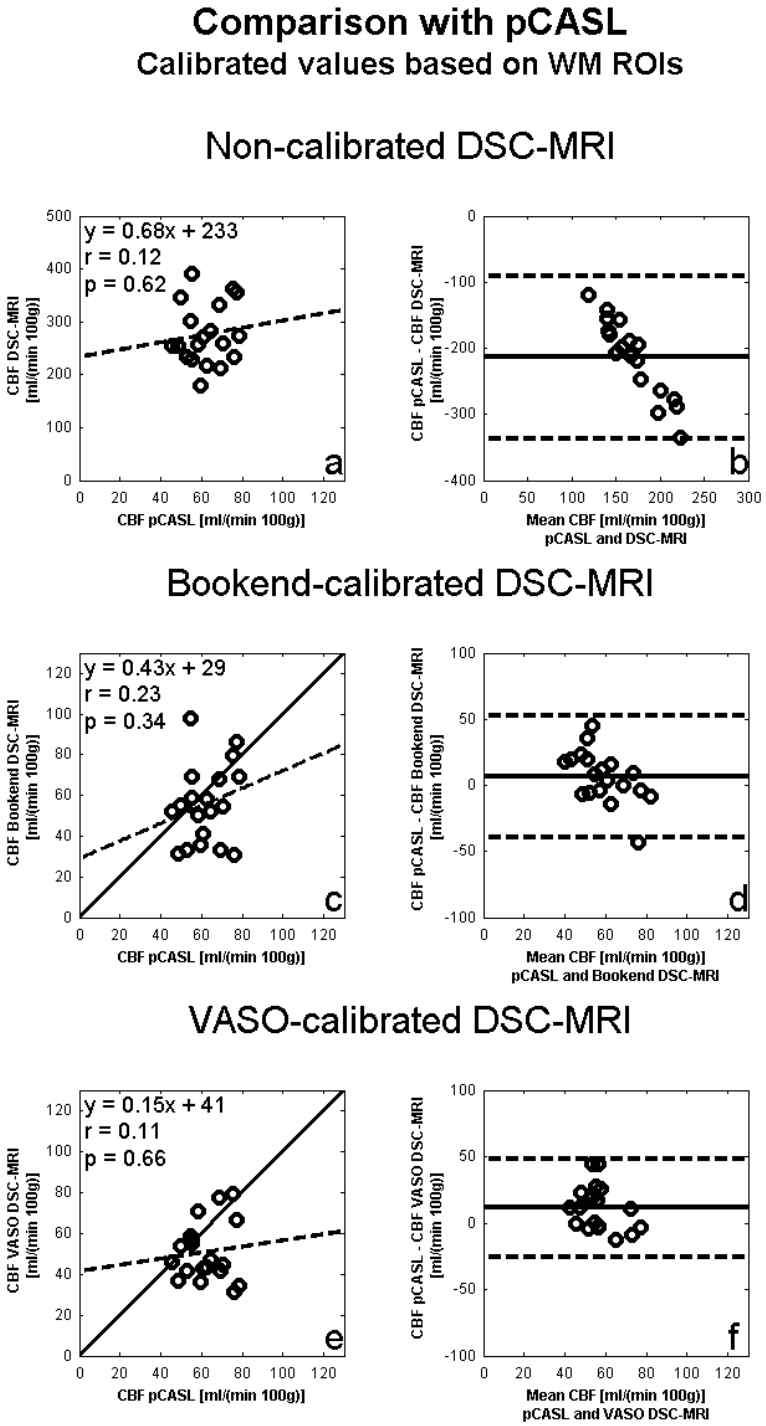

Fig. 5 GM CBF from non-calibrated DSC-MRI and from DSC-MRI calibrated using Bookend and VASO, all compared with pCASL. The calibrated values are based on $CBV_{reference}$ from WM ROIs. Data represent mean values of visit 1 and visit 2 for each volunteer. Solid lines in the scatter plots show the identity line and dotted lines indicate the results from the linear regression. The solid lines in the Bland-Altman plots show the mean difference between pCASL and DSC-MRI and the dotted lines show mean$\pm 1.96 \cdot SD_c$

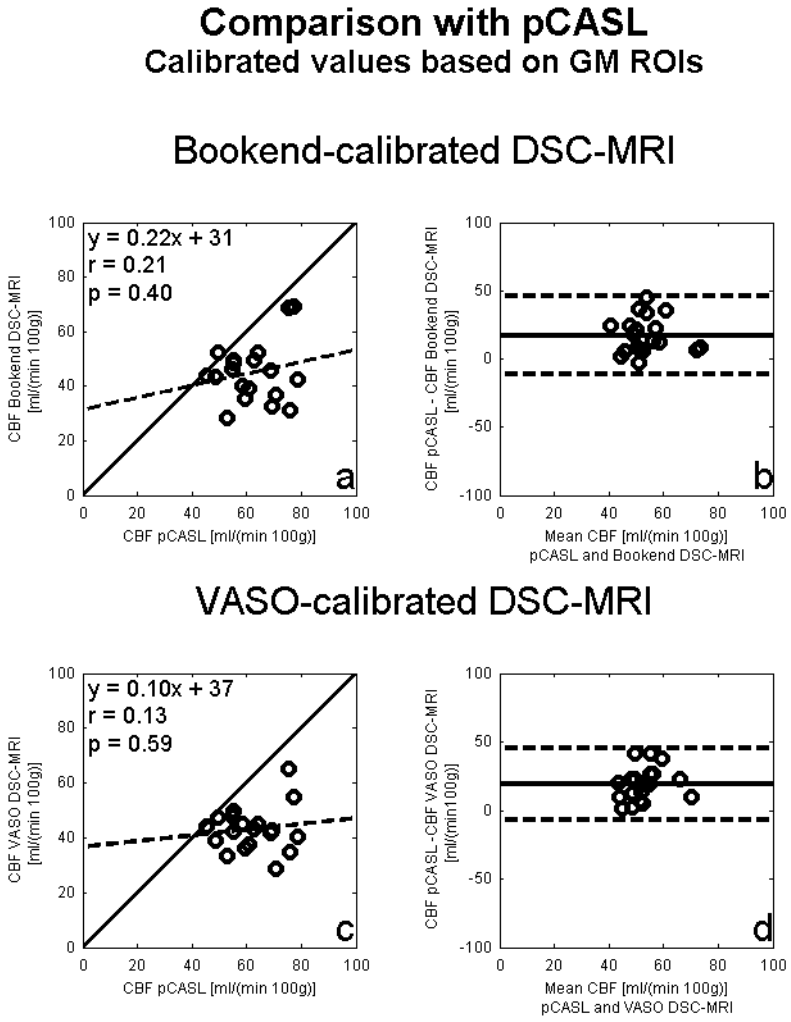

Fig. 6 Comparison between DSC-MRI (calibrated using Bookend and VASO) and pCASL. GM ROIs for extracting GM CBF values are the same as in Figure 5, but calibration factors are based on $CBV_{reference}$ from GM ROIs. The mean value of visit 1 and 2 are used. The identity line is shown as solid lines in the scatter plots and the results from the linear fit are shown as dotted lines. Bland-Altman plots show the mean values of the differences between the methods in the solid lines and mean$\pm 1.96 \cdot SD_c$ in the dotted lines

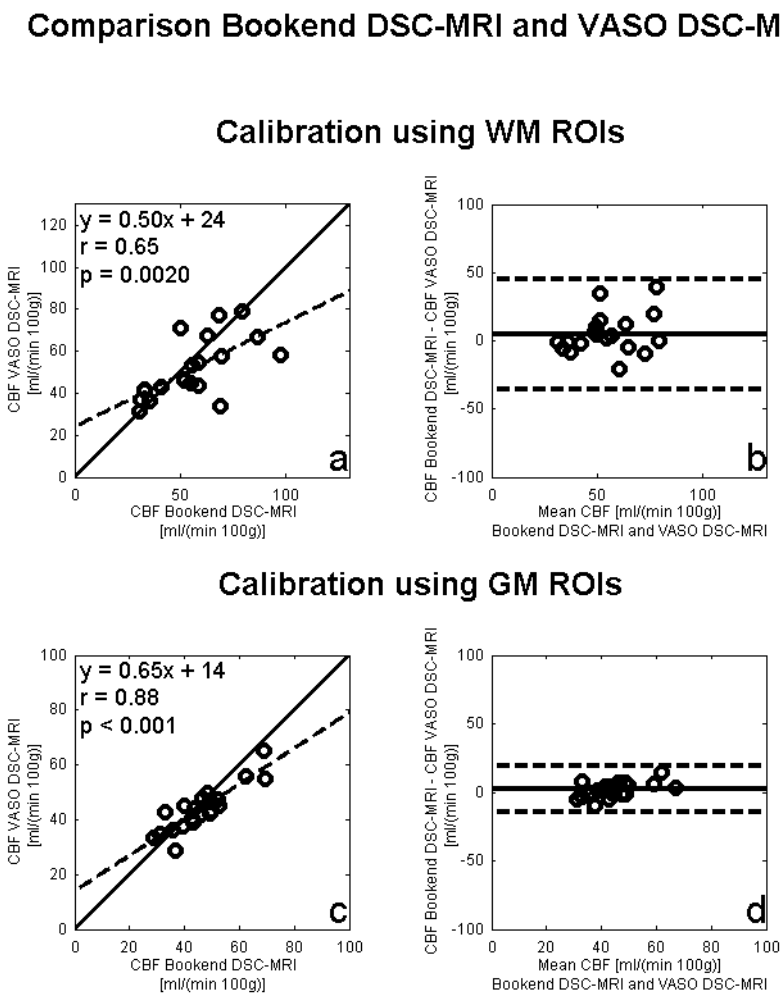

Fig. 7 Comparison of VASO and Bookend with regard to GM CBF. The calibration factors for VASO and Bookend are based on $CBV_{reference}$ from (a-b) WM ROIs and (c-d) GM ROIs. The identity line is shown as solid lines and the linear fit as dotted lines in the scatter plots. In the Bland-Altman plots, the solid lines show the mean difference between VASO and Bookend and the dotted lines show mean$\pm 1.96 \cdot SD_c$

Table 1. Timing for the imaging protocol. Indicated delays between sequences are due to other sequences in the protocol, not used in this particular project, and additional time delays are not included

Starting time (min:sec)	Duration	Sequence
0:0	0:50	M0 for pCASL
0:50	4:04	pCASL
15:08	2:36	Pre-CA VASO
17:44	4:00	Pre-CA T1
24:52	1:31	DSC-MRI with CA injection
28:17	4:00	Post-CA T1
33:47	2:36	Post-CA VASO

Table 2. Grey matter CBF values obtained using non-calibrated DSC-MRI, VASO- and Bookend-calibrated DSC-MRI and pCASL. Calibration factors are based on WM ROIs

	Grey matter CBF (mean±SD) **[ml/(min 100g)]**
Non-calibrated DSC-MRI	277±61 (n=40)
DSC-MRI calibrated using Bookend	56±23 (n=40)
DSC-MRI calibrated using VASO	52±16 (n=40)
pCASL	63±11 (n=36)